*designs*

**MDPI**

*Article*

# Testing System for PV Grid-Connected Power Condition Systems with Support for Ancillary Services

**Vitor Fernão Pires** [1,2,3], **Armando Cordeiro** [2,3,4], **Daniel Foito** [1,2,5], **João F. Martins** [5,6], **Armando Pires** [1,2,5,*] **and Hao Chen** [7]

1 ESTSetúbal, DEE, IPS—Instituto Politécnico de Setúbal, 2910-761 Setúbal, Portugal
2 Sustain.RD, IPS—Instituto Politécnico de Setúbal, 2914-508 Setúbal, Portugal
3 INESC-ID, Lisboa, 1000-029 Lisboa, Portugal
4 ISEL, DEEEA, IPL—Instituto Politécnico de Lisboa, 1959-007 Lisboa, Portugal
5 UNINOVA-CTS, UNL, 2829-516 Caparica, Portugal
6 FCT, DEEC, UNL—Universidade Nova de Lisboa, 2829-516 Caparica, Portugal
7 School of Electrical Engineering, China University of Mining and Technology, Xuzhou 221000, China
* Correspondence: armando.pires@estsetubal.ips.pt (A.P.)

**Abstract:** Due to the high spread of photovoltaic (*PV*) systems in the low voltage distribution grids there is a substantial number of requirements for the connection of these systems. Therefore, several tests should be performed before the integration of the *PV* systems into the grid. Moreover, new requirements have been established that are most likely to be implemented in the near future. To provide these tests and verify if *PV* systems are in accordance with requirements and recommendations, a testing setup for the *PV* systems was developed. This testing system consists of a controllable power source prepared to receive energy and to inject it into the grid. In fact, that system imposes a controllable voltage, in amplitude and frequency, to the *PV* system to simulate the perturbations of the grid. Since the system under test must inject energy in accordance with the standards' specifications, then the controllable power source that emulates the grid must receive that energy. Moreover, it should also be prepared for *PV* systems that are able to provide ancillary services, including new ones that support imbalanced networks. A fast and robust control system will be used for this controllable power source. Several experimental tests from the developed prototype are presented.

**Keywords:** photovoltaic system; *PV* standards; testing system; ancillary services

## 1. Introduction

The importance of producing sustainable electrical energy is nowadays recognized as fundamental due to environmental problems such as global warming and air pollution. The production of electrical energy from renewable energy sources is the path to achieve this desired goal. Among the several renewable energy sources, *PV* generators are now recognized as one of the most important and with high possibilities of great growth [1–3]. However, the integration of the *PV* generators into the distribution grids requires that their power condition system should take into consideration several issues, such as the ones related with grid injected harmonic currents, other power quality issues, islands and the capability to provide ancillary services [4–6]. There are several standards for *PV* interconnection, the most known being published by the Institute of Electrical and Electronics Engineers (*IEEE*) and International Electrotechnical Commission (*IEC*), although several National Standards should also be considered [7]. Under these circumstances *PV* generators should be subject to extended tests.

The importance of testing the *PV* generators leads to the development of several types of testing systems. One of these systems is the so-called *PV* emulator that allows substituting the *PV* arrays and testing the *PV* inverter in an easy way for different testing conditions (associated with solar irradiation and temperature). This kind of emulator

behaves as a controlled source emulating the *PV* array characteristic. This controlled source allows emulating the I-V and *PV* characteristics of a specific *PV* array considering several ambient factors. There are two types of controlled voltage sources: the linear power amplifier [8–14] and the switch mode power converter [15–20]. One aspect that is critical in these emulators is the use of the *PV* model that can be more or less complex [21–28]. For example, one aspect that is not considered in many emulators is a model in which the nonlinear dynamic characteristics bias region, in both forward and reverse, is used [29]. Regarding the linear power amplifier, this presents a very high dynamic performance. However, its efficiency is low, being not indicated for medium- and high-power applications. On the other hand, the switch mode power converter presents several advantages, such as high efficiency, high power density and low cost, being indicated for medium- and high-power applications. Another aspect associated with the PV panels testing is regarding arc faults that are one of three major failures in PV systems. Thus, detectors for this kind of fault are required by, for example, the National Electric Code and Underwriters Laboratories standard 1699B. Thus, a testing system for this kind of fault was also proposed [30]. This system was developed specifically for PV systems since this kind of fault is different when compared with AC-system arc fault detectors.

Regarding the test for the *PV* grid-connected power condition systems, a grid emulator that will allow verifying if the standards and other requirements are met should be used. This grid emulator must be connected, preferably to the grid, in order to transfer the generated active power by the *PV* array. Several grid emulators have been developed [31–34]. However, these emulators have been specifically developed to study classical power systems (such as protection relays, industrial equipment and transformers), wind turbines and wave energy converters [35–40]. Several types of grid emulators were proposed in the past, namely, the linear power amplifier based, the transformer based and the switch mode power amplifier based. The first one presents a very high dynamic performance, but is very expensive and is characterized by a high volume and weight. The second type (transformer based) is very limitative since only can generate *AC* voltages with different amplitudes [41]. Regarding the switch mode power amplifier based, it is a very competitive solution since it is characterized by high efficiency, high power density and low cost. However, the opposite of what has been executed regarding the *PV* emulator, specially developed for *PV* grid-connected power condition systems, have not been reported. These systems have specific requirements that are not associated with other power system components. In fact, the emulator must be prepared for any kind of *PV* inverter, both from the point of view of its topology and its control [42–51]. Moreover, new ancillary services, such as the support to imbalanced networks is expectable in the future, and this has also been considered.

This work seeks to present a testing system specially designed for *PV* grid-connected power condition systems. The proposed testing system includes a four-wire voltage source inverter in the power conversion stage with the purpose of allowing ancillary services that support imbalanced networks. Additionally, a fast and robust current control system to ensure the desired dynamic response of the testing system is also proposed. In this way, it is ensured that the proposed system is useful to be used as a testing system in real applications. The control system consists of a voltage and current controller to regulate the output voltage of the power converter in the desired reference in a very fast way. A laboratory prototype was developed in this way to test real *PV* grid-connected power condition systems with support for ancillary services.

Regarding the structure of this paper, it consists of six sections, this one being the introduction. In the second section, the problems related to the connection of a PV system to the grid and the requirements that already exist to avoid that are mentioned. The third section presents the proposed testing systems and the power electronic converters. The control strategy for the power electronic converters used in the proposed testing system are presented in section four. The experimental results obtained with this experimental system are presented in section five. In section six, a discussion of this kind of testing systems is

presented. Finally, the conclusions of the work and some perspectives are presented in section seven.

## 2. Requirements for *PV* Grid-Connected Power Conditions Systems

Connecting a *PV* system to the grid may affect the effectiveness of the power system, either in transient mode or on steady state mode. The safe and trusted grid connection of several *PV* systems remains a huge challenge in today's modern grid developments and their connection most likely presents side effects that demand particular attention. Amongst others, the effects of connecting *PV* systems to the grid could include voltage problems, harmonic distortion problems, power factor, *DC* current injection or island operation [52–54]. To further reinforce grid stability and reliability, the European Network of Transmission System Operators for Electricity (ENTSO-E) has defined precise rules that are applicable to all types of grid-connected generators. Typically, grid-connected *PV* systems are only considered for standard operation under the three following conditions: (a) continuous operation, where they operate at nominal voltage and frequency levels (with some small tolerance); (b) constrained operation, where curtailment or DSO imposed power set points are considered; and (c) disconnection, where they should stop power injection.

There are a huge number of applicable grid codes, and usually those rules differ from country to country, which is a strong barrier regarding grid-connected *PV* system's large deployment [55–58]. The system described in this paper presents the strong advantage of being fully parameterized, thus country-independent, and capable of being used for every grid code in every country.

One important aspect of the grid codes associated to the problem of grid blackouts is due to the fact that power generator systems starts to disconnect under a problem that appears in the grid. To avoid this problem, several grid-code regulations appear with the purpose to maintain renewable energy sources (such as the wind and *PV* generators) connected to the grid during a specific time when the voltage drops. This specification is usually known as low-voltage ride-through (LVRT). Several countries such as Germany, China and the US among others proposed standards associated with this. Some of the standards that can be referred are the IEEE 1547, GB/T 19964, Q/GDW 617, GB/T 29319 and VDE AR N4105. Another aspect is related to the voltage fluctuation. In this context, there are standards such as IEC 61727 and IEEE 1547 that do not impose a voltage level for *PV* systems. However, Korea KEPCO Technical Guidelines impose limitations either on the short or long term (less than 4% in 2 s fluctuations). When considering the power factor, the majority of the standards impose a minimum of 0.9. Additionally, as an example, IEC 61727 impose 50% of the *PV* system nominal power as minimum power to be injected into the grid. Power quality is highly affected by harmonic distortion caused by *PV* systems. IEC 61727 and IEEE 929 impose a maximum of current distortion for odd harmonics below the 9th order and a maximum of 5% for the total harmonic distortion. Most regulations and connection standards also demand that a *PV* system detects island situations and stop power injection in those circumstances. IEC 61727 and IEEE 1547 impose 2 s as stop time after island appears, and a maximum of 5 min to reconnect after normal grid conditions are established.

If proper measures are not considered, *PV* systems inverters could inject a current *DC* component into the grid, leading, for example, to distribution transformers overheating due to asymmetrical magnetization levels. IEC 61727 imposes a maximum of 1% of the rated output current while IEEE 1547 or IEEE 929 impose a maximum of 0.5%. Voltage imbalance limits are quite different from country to country. Nevertheless, the 2% limit is usually considered. Regarding power imbalance, the German "Power Generating Plants Connected to the Low-voltage Grid" Code of Practice (E VDE-AR-N 4105) [59] considers a maximum of 4.6 kVA of power imbalance between the three phases for a maximum installed power of single phase 10 kVA. Thus, to eliminate or attenuate this problem of imbalance, it has been considered and studied with the implementation of four-wire *PV*

inverters [60]. In this case, it will be possible to inject an imbalanced active power by the *PV* systems in a way that will compensate the load grid imbalance.

## 3. Description of the Proposed Testing System

As described in the previous section, there are nowadays many standards that impose or recommend specifications for the *PV* systems connected to the grid. There are also new recommendations addressing new functions, such as the reactive power control and power factor regulation and the load balance through the injection of imbalanced active and reactive powers. To test *PV* systems in accordance with those specifications and studies, an adapted testing system was designed. A simplified block diagram of the overall system is presented in Figure 1. The overall system under test consists of *PV* panels, power condition system (that integrates the *MPPT*, and *DC-AC* converter), batteries (optional), testing system and grid. Associated with the testing system, there is a communication module, allowing for connecting the testing system to a computer in order to receive signals and program the required tests.
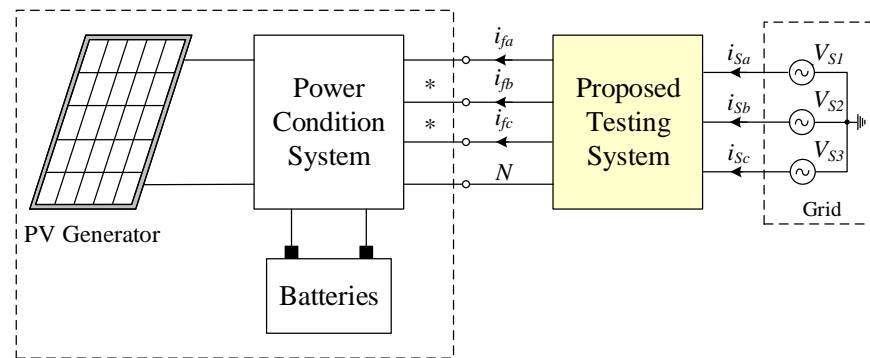


**Figure 1.** Simplified block diagram of the overall system (single phase without *phases or three-phase with *phases).

Regarding the testing system, a Back to Back system was adopted to allow bidirectional energy transfer. For the power converter connected to the grid, a three-leg three-phase voltage source inverter was adopted. However, for the power converter connected to the *PV* systems, a four-leg three-phase voltage source inverter that allows for testing the system in conditions such as transfer of the energy in an imbalanced way to provide ancillary services such as the support of the imbalanced networks was adopted. A *LC* low pass filter is connected to the output of this converter. Figure 2 shows the power circuit of the proposed testing system.
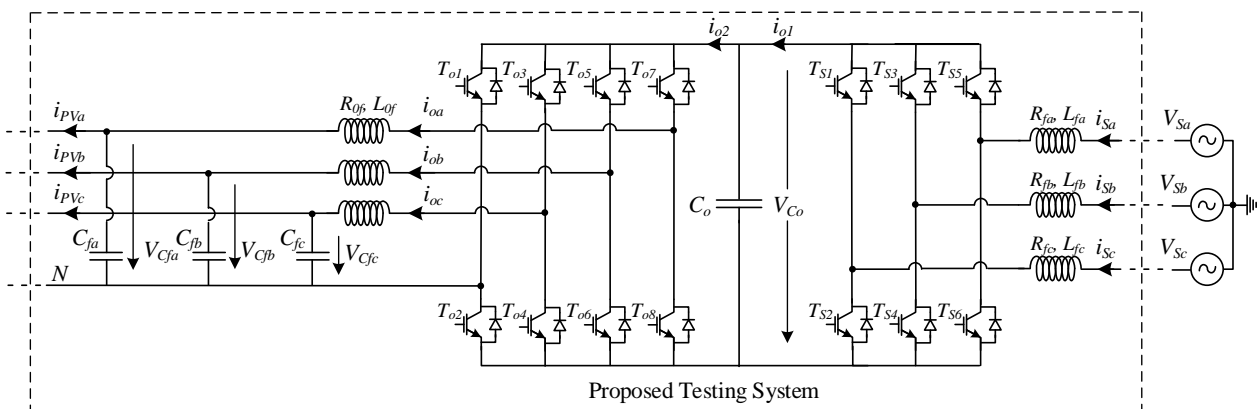


**Figure 2.** Power circuit configuration of the proposed *DC-DC* converter for transformerless *PV* applications.

The proposed system will be able to test the *PV* generators even in conditions of imbalance or in a distortion mode; however, it will transfer the energy to the grid in a balanced mode and with a near-unity power factor.

## 4. Control Strategy for the PV System

As verified in the previous section, the *PV* testing system must be controlled taking into consideration two sides: the grid side, and the connection to the *PV* power condition system. Thus, the power converter associated to the grid side (rectifier part) will be controlled with the purpose of regulating the *DC* voltage bus. The power converter will transfer the energy from or to the grid depending on if the *DC* voltage is lower or higher than its reference value. On the other hand, the power converter associated to the *PV* system under test will be controlled in order to behave as a grid in which the parameters could be defined in accordance with the required tests. For the development of the control systems, the mathematical model of the correspondent power circuits is required. Thus, these models are obtained from the state-space equations that allow for describing the dynamic behavior of the testing system. Considering the power circuit of Figure 2, the correspondent displayed state variables and applying Kirchhoff's voltage law, those equations are:

$$\begin{bmatrix} v_{R_a} \\ v_{R_b} \\ v_{R_c} \end{bmatrix} = \begin{bmatrix} v_{S_a} \\ v_{S_b} \\ v_{S_c} \end{bmatrix} - R_f \begin{bmatrix} i_{S_a} \\ i_{S_b} \\ i_{S_c} \end{bmatrix} - L_f \frac{d}{dt} \begin{bmatrix} i_{S_a} \\ i_{S_b} \\ i_{S_c} \end{bmatrix} \tag{1}$$

$$\begin{bmatrix} v_{C_a} \\ v_{C_b} \\ v_{C_c} \end{bmatrix} = \begin{bmatrix} v_a \\ v_b \\ v_c \end{bmatrix} - R_{of} \begin{bmatrix} i_{fa} \\ i_{fb} \\ i_{fc} \end{bmatrix} - L_{of} \frac{d}{dt} \begin{bmatrix} i_{fa} \\ i_{fb} \\ i_{fc} \end{bmatrix} \tag{2}$$

$$\frac{d}{dt} \begin{bmatrix} v_{C_o} \\ v_{C_{fa}} \\ v_{C_{fb}} \\ v_{C_{fc}} \end{bmatrix} = \begin{bmatrix} \frac{1}{C_o} & 0 & 0 & 0 \\ 0 & \frac{1}{C_f} & 0 & 0 \\ 0 & 0 & \frac{1}{C_f} & 0 \\ 0 & 0 & 0 & \frac{1}{C_f} \end{bmatrix} \begin{bmatrix} i_{o1} \\ i_{fa} \\ i_{fb} \\ i_{fc} \end{bmatrix} - \begin{bmatrix} \frac{1}{C_o} & 0 & 0 & 0 \\ 0 & \frac{1}{C_f} & 0 & 0 \\ 0 & 0 & \frac{1}{C_f} & 0 \\ 0 & 0 & 0 & \frac{1}{C_f} \end{bmatrix} \begin{bmatrix} i_{o2} \\ i_{PV_a} \\ i_{PV_b} \\ i_{PV_c} \end{bmatrix} \tag{3}$$

The pole voltages of each of the converters ($v_{R_{a,b,c}}$ and $v_{a,b,c}$) are functions of the switches' state and the *DC* link voltage. These voltages are described by Equations (4) and (5), considering that the switches are represented by binary variables ($\gamma$ for three-leg converter and $\delta$ for four-leg converter), where 1 is for upper switch *ON* and lower *OFF* and 0 is for the vice versa condition.

$$\begin{bmatrix} v_{R_a} \\ v_{R_b} \\ v_{R_c} \end{bmatrix} = \begin{bmatrix} \gamma_a \\ \gamma_b \\ \gamma_c \end{bmatrix} v_{C_o} \tag{4}$$

$$\begin{bmatrix} v_{C_a} \\ v_{C_b} \\ v_{C_c} \end{bmatrix} = \begin{bmatrix} \delta_a \\ \delta_b \\ \delta_c \end{bmatrix} v_{C_o} \tag{5}$$

For the implementation of the control system, an approach is used that will be based on the $\alpha\beta o$ coordinates. To develop this control system, taking this into consideration, obtaining the system model in $\alpha\beta o$ coordinates is required. Hence, the equations of the system in these coordinates ($\alpha\beta o$) are given by Equation (6), where Equation (7) is the Clarke-Concordia transform [61].

$$\begin{cases} v_{R_{\alpha\beta}}, i_{S_{\alpha\beta}} = T_{\alpha\beta} \, v_{R_{a,b,c}}, \, T_{\alpha\beta} \, i_{S_{a,b,c}} \\ v_{C_{\alpha\beta o}}, i_{f_{\alpha\beta o}} = T_{\alpha\beta o} \, v_{C_{a,b,c}}, \, T_{\alpha\beta o} \, i_{f_{a,b,c}} \end{cases} \tag{6}$$

$$T_{\alpha\beta o} = \sqrt{\frac{2}{3}} \begin{bmatrix} 1 & -\frac{1}{2} & -\frac{1}{2} \\ 0 & \frac{\sqrt{3}}{2} & -\frac{\sqrt{3}}{2} \\ \frac{1}{2} & \frac{1}{2} & \frac{1}{2} \end{bmatrix} \tag{7}$$

The state-space representation of this system, considering $\alpha\beta o$ coordinates, will then be given by Equations (8) and (9):

$$\frac{d}{dt} \begin{bmatrix} i_{S_\alpha} \\ i_{S_\beta} \\ i_{f_\alpha} \\ i_{f_\beta} \\ v_{C_o} \end{bmatrix} = \begin{bmatrix} -\frac{R_f}{L_f} & 0 & 0 & 0 & -\frac{\gamma_\alpha}{L_f} \\ 0 & -\frac{R_f}{L_f} & 0 & 0 & -\frac{\gamma_\beta}{L_f} \\ 0 & 0 & -\frac{R_{of}}{L_{of}} & 0 & -\frac{\delta_\alpha}{L_{of}} \\ 0 & 0 & 0 & -\frac{R_{of}}{L_{of}} & -\frac{\delta_\beta}{L_{of}} \\ \frac{\gamma_\alpha}{C_o} & \frac{\gamma_\beta}{C_o} & -\frac{\delta_\alpha}{C_o} & -\frac{\delta_\beta}{C_o} & 0 \end{bmatrix} \begin{bmatrix} i_{S_\alpha} \\ i_{S_\beta} \\ i_{f_\alpha} \\ i_{f_\beta} \\ v_{C_o} \end{bmatrix} + \begin{bmatrix} \frac{1}{L_{of}} & 0 & 0 & 0 \\ 0 & \frac{1}{L_{of}} & 0 & 0 \\ 0 & 0 & \frac{1}{L_{of}} & 0 \\ 0 & 0 & 0 & \frac{1}{L_{of}} \\ 0 & 0 & 0 & 0 \end{bmatrix} \begin{bmatrix} v_{S_\alpha} \\ v_{S_\beta} \\ v_{C_{f\alpha}} \\ v_{C_{f\beta}} \end{bmatrix} \tag{8}$$

$$\frac{d}{dt} \begin{bmatrix} v_{C_{f\alpha}} \\ v_{C_{f\beta}} \end{bmatrix} = \begin{bmatrix} \frac{1}{C_{of}} & 0 \\ 0 & \frac{1}{C_{of}} \end{bmatrix} \begin{bmatrix} i_{f_\alpha} \\ i_{f_\beta} \end{bmatrix} - \begin{bmatrix} \frac{1}{C_{of}} & 0 \\ 0 & \frac{1}{C_{of}} \end{bmatrix} \begin{bmatrix} i_{PV_\alpha} \\ i_{PV_\beta} \end{bmatrix} \tag{9}$$

In this system, the variables under control are the input currents of the three-leg converter ($i_{sa}$, $i_{sb}$ and $i_{sc}$), the capacitor voltage of the *DC* bus ($v_{Co}$) and the three-phase capacitor voltages associated to the four-leg converter ($v_{Cfa}$, $v_{Cfb}$, $v_{Cfc}$). However, the reference of the *AC* currents of the converter connected to the grid (three-leg inverter) will be defined by the controller associated to the *DC* bus. On the other hand, the controller associated to the *PV* systems (four-leg inverter) will be independent of the other system to ensure the desirable characteristics that are required for the applied voltage. With the purpose of obtaining a robust controller for the *AC* voltages and currents, controllers based on the variable structure control are adopted. However, for the activation of the switches of both converters, $\alpha\beta o$ vectorial modulators will be used (or $\alpha\beta o$ for the four-leg inverter). Hence, the control equations will be defined in the $\alpha\beta o$ plane (or $\alpha\beta o$ for the four-leg inverter). Taking into consideration the state space model of the converters in the controllability canonical form and the feedback errors, the control equations are defined by Equations (10) and (11) [62]:

$$\begin{cases} S_{i_{s\alpha}} = k_i \left( i_{s_\alpha ref} - i_{s_\alpha} \right) \\ S_{i_{s\beta}} = k_i \left( i_{s_\beta ref} - i_{s_\beta} \right) \end{cases} \tag{10}$$

$$\begin{cases} S_{v_{Cof\alpha}} = \left( v_{C_{of\alpha}ref} - v_{C_{of\alpha}} \right) + k_v \left( \frac{dv_{C_{of\alpha}ref}}{dt} - \frac{dv_{C_{of\alpha}}}{dt} \right) \\ S_{v_{Cof\beta}} = \left( v_{C_{of\beta}ref} - v_{C_{of\beta}} \right) + k_v \left( \frac{dv_{C_{of\beta}ref}}{dt} - \frac{dv_{C_{of\beta}}}{dt} \right) \\ S_{v_{Co}} = \left( v_{C_o ref} - v_{C_o} \right) + k_v \left( \frac{dv_{C_o ref}}{dt} - \frac{dv_{C_o}}{dt} \right) \end{cases} \tag{11}$$

From the last control Equation (11) is possible to see that the control is dependent on the derivate of the capacitor voltages. However, under the point of view of a real application, this can be a problem since normally there is noise associated with the acquired signals. Hence, through Kirchhoff's current law, the derivate of the capacitor voltages could be replaced by the inductor and *PV* system currents, leading to a new control law as described by Equation (12).

$$\begin{cases} S_{v_{Cof\alpha}} = \left( v_{C_{of\alpha}}ref - v_{C_{of\alpha}} \right) + k_v \left( \frac{dv_{C_\alpha ref}}{dt} - \frac{i_{f_\alpha} - i_{PV_\alpha}}{C_f} \right) \\ S_{v_{Cof\beta}} = \left( v_{C_{of\beta}}ref - v_{C_{of\beta}} \right) + k_v \left( \frac{dv_{C_{of\beta}ref}}{dt} - \frac{i_{f_\beta} - i_{PV_\beta}}{C_f} \right) \\ S_{v_{Co}} = \left( v_{C_o ref} - v_{C_o} \right) + k_v \left( \frac{dv_{C_o ref}}{dt} - \frac{\gamma_\alpha i_{s_\alpha} + \gamma_\beta i_{s_\alpha} - \delta_\alpha i_{f_\alpha} - \delta_\beta i_{f_\beta}}{C_o} \right) \end{cases} \tag{12}$$

By the analysis of the control law associated to the control of the *DC* voltage of the two inverters, a problem related with this nonlinear system is verified. This problem is associated with the sliding function that controls the *DC* voltage of the two inverters since include the nonlinear terms $\gamma_\alpha$, $\gamma_\beta$, $\delta_\alpha$ and $\delta_\beta$. Thus, using a transformation from the referential $\alpha\beta$ to the referential $dq$ applying the transform given by Equation (13), a new sliding surface is obtained in accordance with Equation (14) [61].

$$T_{dqo} = \begin{bmatrix} \cos(\theta) & \sin(\theta) & 0 \\ -\sin(\theta) & \cos(\theta) & 0 \\ 0 & 0 & 1 \end{bmatrix} \tag{13}$$

$$S_{v_{Co}} = \left(v_{C_oref} - v_{C_o}\right) + k_v \left(\frac{dv_{C_oref}}{dt} - \frac{\gamma_d i_{S_d} + \gamma_q i_{S_q} - \delta_d i_{f_d} - \delta_q i_{f_q}}{C_o}\right) \tag{14}$$

This can be solved considering: (a) the power balance equations are in steady-state, (b) that the converter connected to the grid only exchanges active power, and (c) that the mean value of the capacitor current in steady state is zero. In agreement with these three considerations, the following relationships are obtained:

$$\begin{cases} v_{Co}i_{o1} \approx v_{S_d}i_{S_d} + v_{S_q}i_{S_q} \\ v_{Co}i_{o2} \approx v_{C_{fd}}i_{f_d} + v_{C_{fq}}i_{f_q} \\ \gamma_d i_{S_d} + \gamma_q i_{S_q} \approx i_{o1} \\ \delta_q i_{f_d} + \delta_q i_{f_q} \approx i_{o2} \end{cases} \tag{15}$$

Using the relationships given by Equation (15) and considering that in the Park rotating reference frame $v_{S_q} = 0$, a new sliding surface associated to the control of the *DC* voltage of the two inverters will be obtained, as expressed by Equation (16):

$$S_{v_{Co}} = \left(v_{C_oref} - v_{C_o}\right) + k_v \left(\frac{dv_{C_oref}}{dt} - \frac{v_{S_d}i_{S_d} - v_{C_{fd}}i_{f_d}}{v_{C_o}C_o}\right) \tag{16}$$

Taking into account that the sliding surface must be equal to zero, it will be possible to obtain the current d component that the three-leg inverter must ensure to balance the *DC* capacitor voltage. This current component will, in this way, be given by Equation (17):

$$S_{v_{Co}} = \left(v_{C_oref} - v_{C_o}\right) + k_v \left(\frac{dv_{C_oref}}{dt} - \frac{\gamma_d i_{S_d} + \gamma_q i_{S_q} - \delta_d i_{f_d} - \delta_q i_{f_q}}{C_o}\right) \tag{17}$$

This current component will be used as a reference in the sliding surfaces given by Equation (11). However, since sliding surfaces are defined in the referential $\alpha\beta$, this component and the $i_{S_q}$ that will be zero (to ensure that the power absorbed or injected into the grid is only the active) and will be converted to this referential through the inverse of the Clarke-Concordia transform.

To ensure that the variables under control follow the references, the sliding surfaces given by Equations (10) and (12) should be equal to zero. To ensure that those conditions are reached and after that maintained at the sliding surfaces, a reachability condition must be guaranteed. In this way, the conditions that will ensure the reachability condition will be given by Equations (18) and (19) [62]:

$$S_{i\alpha}(e_{i_{s\,\alpha}}, t)\dot{S}_{i\alpha}(e_{i_{s\,\alpha}}, t) < 0 \tag{18}$$

$$S_{i\beta}\left(e_{i_{s\,\beta}}, t\right)\dot{S}_{i\beta}\left(e_{i_{s\,\beta}}, t\right) < 0 \tag{19}$$

The conditions given by Equations (18) and (19) will be ensured through a vectorial modulator that will choose the state of the switches in order to apply the desired voltage.

The *AC* voltages of the two inverters in $\alpha\beta$ and $\alpha\beta o$ coordinates leads to a diagram in which for the three-leg converter there are eight voltage vectors and sixteen for the four-leg converter. Since the testing system should be prepared to test the *PV* system for imbalanced tests, for the four-leg converter, in addition to the vectors in the $\alpha\beta$ plane, the third dimension given by the o component should also be considered. These vectors are presented in Figure 3.
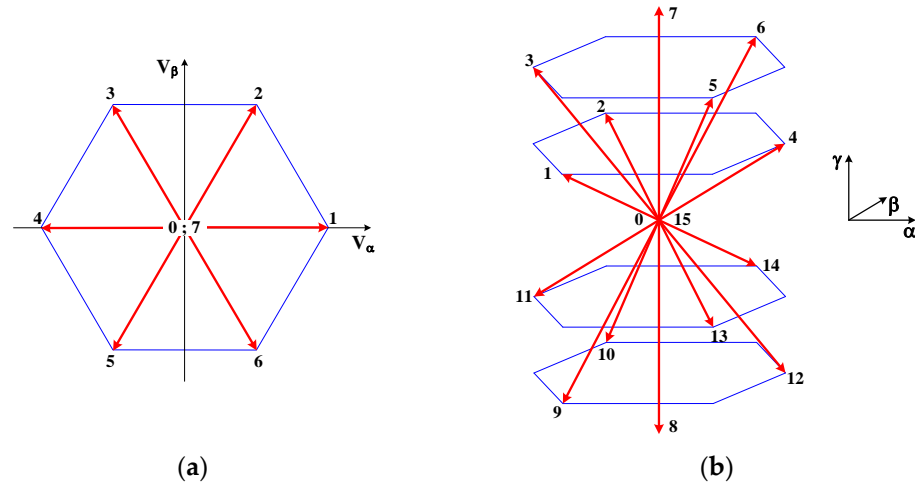


**Figure 3.** Voltage Vectors for the: (**a**) three-leg converter (**b**) four-leg converter.

Taking into consideration converter voltage vectors, it is possible to define conditions to ensure that the trajectory of the sliding surfaces will be in the direction to zero. Consider an example for the three-leg inverter. Assuming, for example, the condition is negative. It should choose a converter voltage vector with a positive $\alpha$ component. For the other component of the sliding surfaces ($S_{i_{s\beta}}$), the same principle should be applied. For the four-leg inverter, the o component should also be considered, since in this inverter the neutral wire is also considered. The implementation of this strategy will be achieved using proper look-up tables. These look-up tables are function of the signal of the sliding surfaces. However, to limit the switching frequency of the power semiconductors between the look-up tables and the result of the sliding surfaces, hysteretic comparators will be used. Given eight and sixteen voltage vectors for the three-leg and four-leg inverters, respectively, hysteretic comparators with three levels are considered (at which their outputs will by $dSi_\alpha$, $dSi_\beta$, $dSv_\alpha$, $dSv_\beta$ and $dSv_o$ that will assume $-1$, 0 or $+1$). Thus, the look-up table for the control system of the three-leg inverter will be given by Table 1, while the four-leg inverter will be given by Table 2. The control system for the three-leg inverter and for the four-leg inverter can be seen in Figures 4 and 5, respectively.
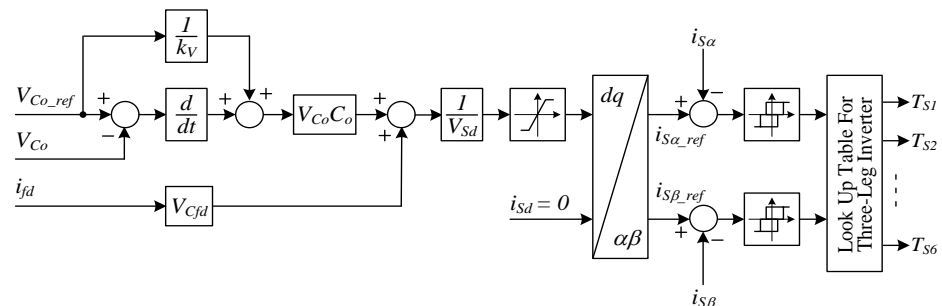


**Figure 4.** Diagram of the current control scheme for the three-leg inverter.

**Table 1.** Adopted Voltage Vectors Function of the Sliding Surfaces for Three-Leg Inverter.

| $dSv_\alpha$ | $dSv_\beta$ | Vector |
|:---:|:---:|:---:|
| −1 | −1 | 5 |
| −1 | 0 | 4 |
| −1 | +1 | 3 |
| 0 | −1 | 5, 6 |
| 0 | 0 | 0, 7 |
| 0 | +1 | 2, 3 |
| +1 | −1 | 6 |
| +1 | 0 | 1 |
| +1 | +1 | 2 |

**Table 2.** Adopted Voltage Vectors Function of the Sliding Surfaces for Four-Leg Inverter.

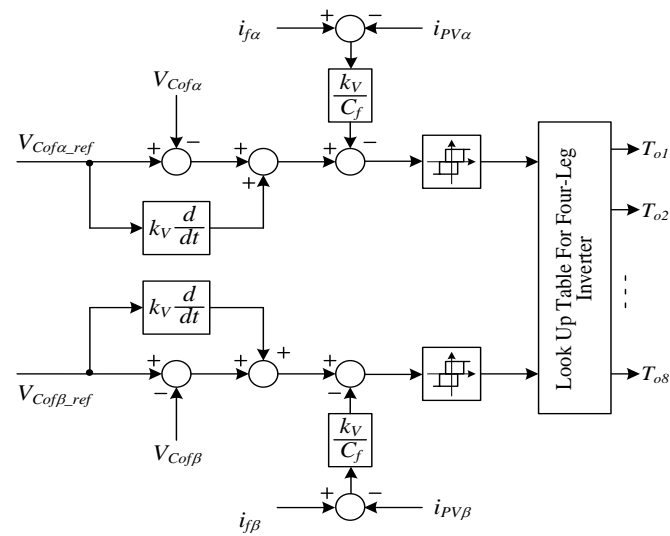| $dSv_\alpha$ | $dSv_\beta$ | $dSv_o$ | Vector |
|:---:|:---:|:---:|:---:|
| −1 | −1 | −1 | 13 |
| −1 | −1 | 0 | 5, 13 |
| −1 | −1 | +1 | 5 |
| −1 | 0 | −1 | 12 |
| −1 | 0 | 0 | 4, 12 |
| −1 | 0 | +1 | 4 |
| −1 | 1 | −1 | 11 |
| −1 | 1 | 0 | 3, 11 |
| −1 | 1 | +1 | 3 |
| 0 | −1 | −1 | 13, 14 |
| 0 | −1 | 0 | 5, 6, 13, 14 |
| 0 | −1 | +1 | 5, 6 |
| 0 | 0 | −1 | 8 |
| 0 | 0 | 0 | 0, 15 |
| 0 | 0 | +1 | 7 |
| 0 | 1 | −1 | 10, 11 |
| 0 | 1 | 0 | 2, 3, 10, 11 |
| 0 | 1 | +1 | 2, 3 |
| 1 | −1 | −1 | 14 |
| 1 | −1 | 0 | 6, 14 |
| 1 | −1 | +1 | 6 |
| 1 | 0 | −1 | 9 |
| 1 | 0 | 0 | 1, 9 |
| 1 | 0 | +1 | 1 |
| 1 | 1 | −1 | 10 |
| 1 | 1 | 0 | 2, 10 |
| 1 | 1 | +1 | 2 |

**Figure 5.** Diagram of the current control scheme for the four-leg inverter.

## 5. Experimental Results

The developed testing system for *PV* generators (in which the inverters are considered) was tested with different systems. For the implementation of this testing system, IGBT's CM100DY 24NF, low-pass filters with 10 mH and 10 μF and input inductors with 10 mH were used. Associated to these power electronic converters, a set of low-power components was considered. These components were designed taking into consideration several aspects, such as the galvanic isolation of the control system and the signal distortion between input and output of the electronic devices [63]. In addition to that, it allows connecting to a laptop with the purpose of choosing the test conditions that will be imposed to the *PV* system under test. This laptop has a program that generates the references for the control system of the power converter and where the user can define the test to be performed. A picture of this testing system is presented in Figure 6. A power quality analyser (Fluke 43B, Fluke Corporation, U.S.) was also used to obtain the values of several parameters, such as active, reactive and apparent power, *THD* and power factor, among others.



**Figure 6.** Prototype of the implemented solar inverter testing system.

The first results that are presented were obtained from a test with a commercial solar inverter, namely, a Solis mini-1000. It is a single-phase inverter with a rated output power of 1000 W. Four solar panels (Solton SPI 60-250P, Solton Power Inc., Chino, CA, USA) were connected to this inverter. Since the *PV* inverter is single phase, only two of the terminals of the proposed testing system ($L_1$ and *N*) were used.

The first test with this commercial solar inverter was performed in steady-state conditions in which the testing system simply applies a single-phase voltage with the nominal value of 230 $V_{RMS}$. The voltage applied by the testing system and the current injected by the solar inverter into this testing system are presented in Figure 7. One aspect that is possible to see is that the injected current presents some distortion. Measuring the *THD* of this current a value of 12.6% was executed. Another aspect is that the current is not perfectly in phase with the voltage. This can be confirmed by the power factor of the system that is 0.79 and the displacement power factor of 0.81 (being the active, reactive and apparent powers of 107 W, 82 VAR and 135 VA, respectively). In this way, the inverter is not only injecting active power but also reactive power. However, when the injected power increases, the *THD* and reactive power reduces. In Figure 8, the voltage applied by the testing system and the current injected by the solar inverter into this testing system is presented again, but for a higher power (the injected power from the *PV* generator changed from 135 VA to 508 VA). The power factor and the displacement power factor increases to 0.99 (being the active, reactive and apparent powers of 503 W, 71 VAR and 508 VA, respectively). The *THD* also was reduced from 12.6% to 4.6%. This shows that the tested *PV* inverter presents a low-power quality when it operates at low-power conditions.
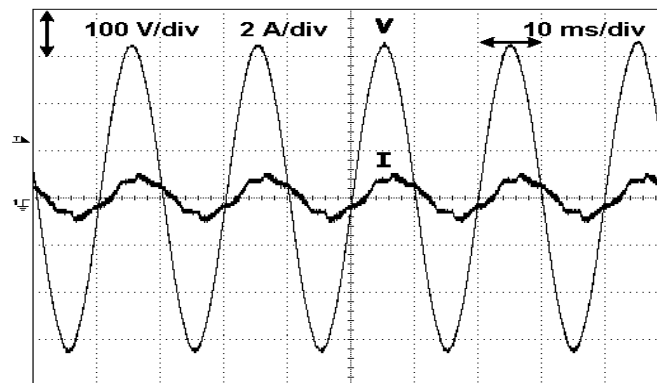


**Figure 7.** Voltage applied by the testing system and current injected by the solar inverter into the testing system when the injected power is 135 VA.
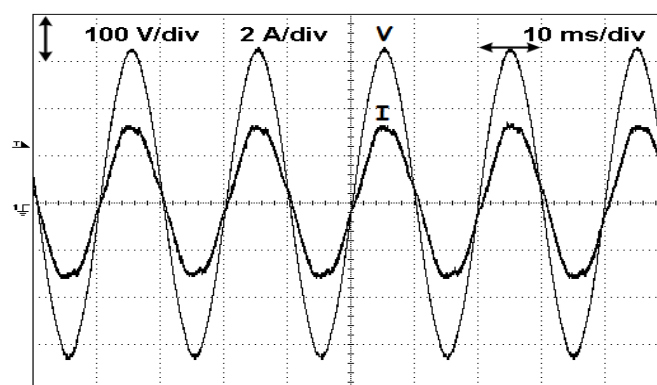


**Figure 8.** Voltage applied by the testing system and current injected by the solar inverter into the testing system when the injected power is 508 VA.

Other tests that were performed with this commercial system addressed voltage sags and *MPPT* operation. A voltage sag of 35% was applied by the testing system to the *PV* system, as presented in Figure 9a. The current injected from the *PV* system to the testing system is presented in Figure 9b. It is possible to see that the *PV* system is immune to this type of voltage sag. Moreover, the operation of the *MPPT* is confirmed, since the *PV* system maintains the value of the injected power (with the reduction in the voltage, the current

increases). However, for voltage sags with higher percentage, the system will disconnect. In Figure 10, a test is presented in which the *PV* testing system started with a voltage with a nominal value and this value was reduced until the *PV* inverter disconnects. From this result, it is possible to confirm that for voltage sags higher than 50%, the inverter will disconnect from the grid.
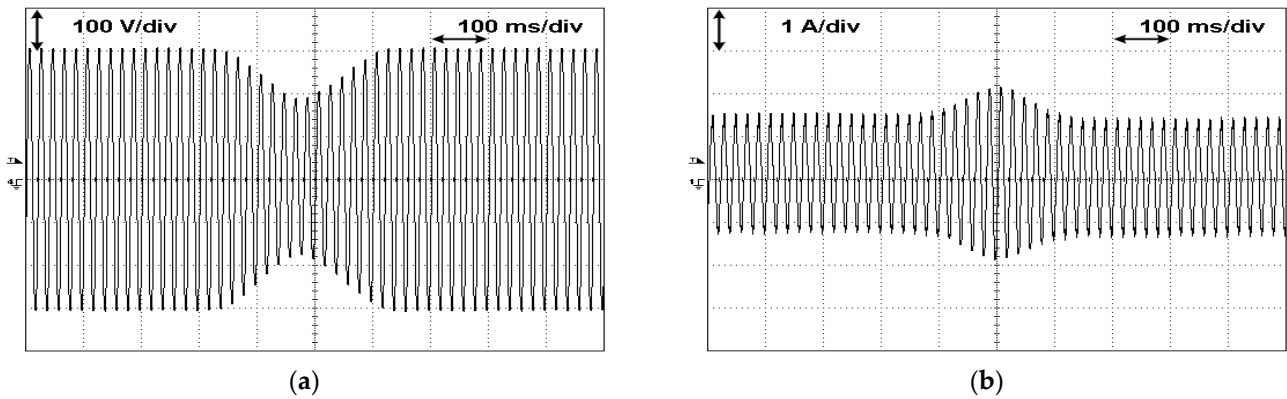


(**a**)



(**b**)

**Figure 9.** Test with a voltage sag: (**a**) output testing system voltage (**b**) current injected by the PV system.
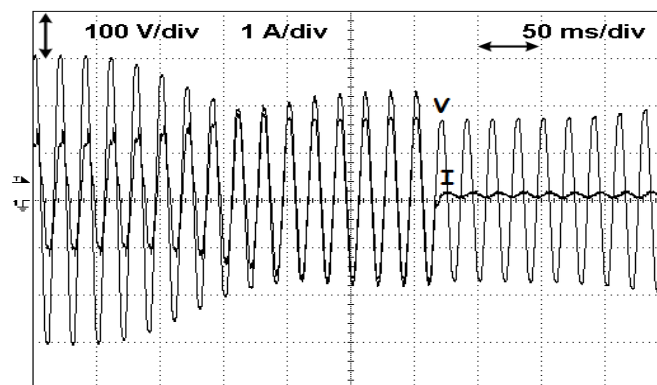


**Figure 10.** Test with a continuous reduction in the output testing system voltage until the *PV* inverter disconnects.

Tests with a three-phase *PV* inverter with four legs were also performed. This system, presented in Figure 11, was developed in the context of a European Project. The purpose of this *PV* inverter was also to give support to low-voltage grids with imbalanced loads.
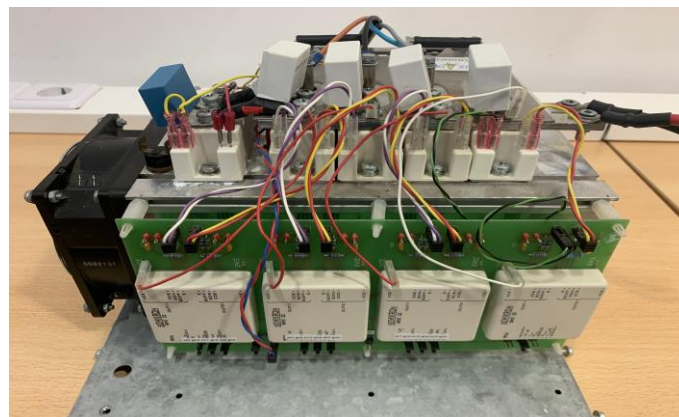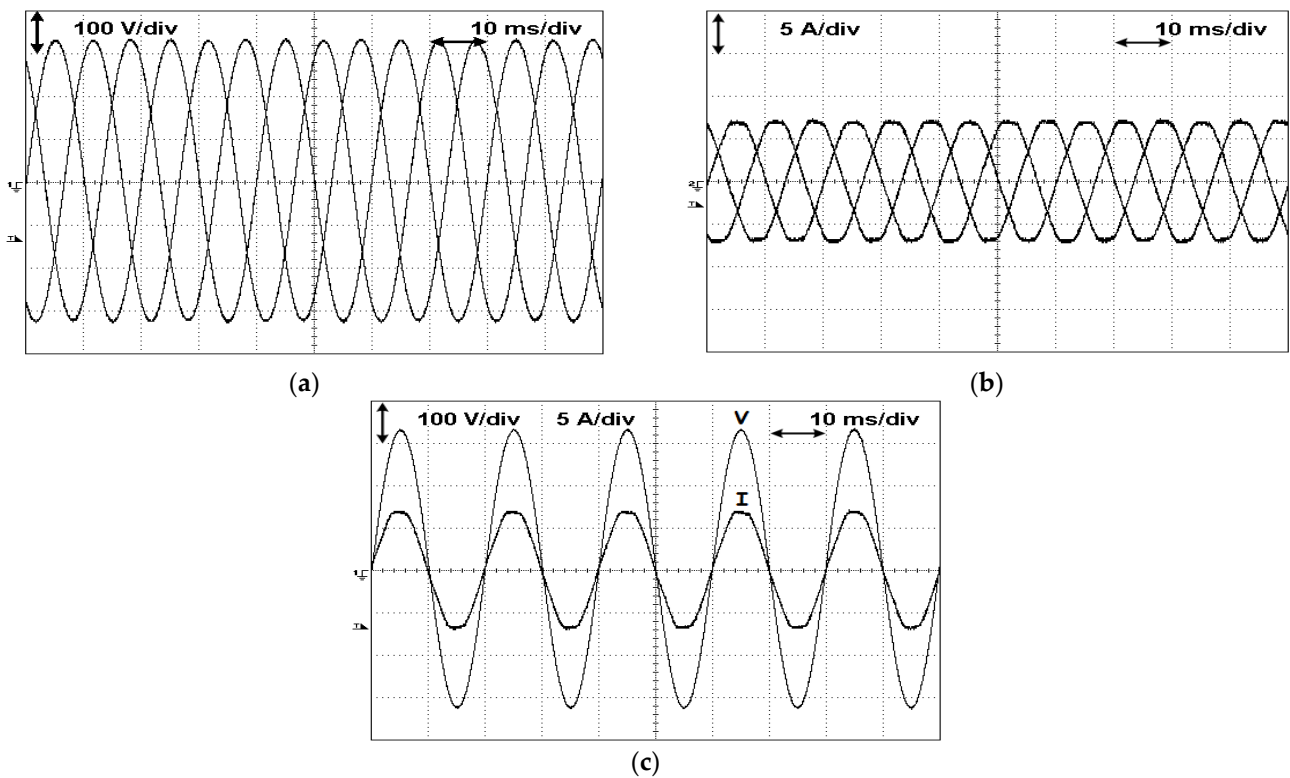


**Figure 11.** Three-phase *PV* inverter with four legs developed in the ambit of a European Project.

The first tests with this three-phase *PV* inverter were performed for grid-balanced conditions. In accordance with the performed tests, the three-phase power supplied from the *PV* inverter to the grid (testing system) is balanced. The three-phase voltages that the testing system imposes on the *PV* inverter are presented in Figure 12a. On the other hand, the three-phase currents of the *PV* inverter are shown in Figure 12b. From those obtained results, it is possible to see that the voltages imposed by the testing system and currents injected by the *PV* inverter are balanced. The *THD* of the currents is also low, with a value of 4.3%. Another important parameter is the power factor that presents a very high value of 0.99 (in this test, the *PV* inverter was set to only inject active power to the grid). This high power factor can also be confirmed by the result shown in Figure 12c, in which the voltage and current in phase $L_1$ of the testing system are presented.



**Figure 12.** Waveforms obtained from the test using the *PV* inverter with four legs for a balanced condition and without reactive compensation: (**a**) three-phase voltages imposed by the testing system, (**b**) three-phase currents injected by the *PV* system, (**c**) voltage and current in phase $L_1$ of the testing system.

One of the ancillary services that has been considered important is the possibility of the *PV* inverter supplying reactive power in order to give support to grids suffering from voltage drop conditions [64]. The inverter under test was designated to provide this service, being the developed testing system used to test this capability. The obtained results in this test can be seen in Figure 13. The voltage and current in phase $L_1$ of the testing system that are presented in Figure 13 show that the current is shifted from the voltage with an angle of around 45°. This confirms that the *PV* inverter is injecting active and reactive power.

A test in which the *PV* inverter provides ancillary services associated to low-voltage grids with imbalanced loads was also performed. In this case, the *PV* inverter operates in a way that injects imbalanced currents to the grid (testing system). In this way, the capability of the *PV* inverter to provide ancillary services to networks with imbalanced loads was tested. The results of this test are shown in Figure 14. From this figure, it is possible to see that although the voltages that the testing system applies are balanced, the injected currents from the *PV* inverter are imbalanced. This test was performed for a condition in which the

*PV* inverter does not provide reactive power. This can be confirmed through Figure 14a, where it is possible to see the near-unity power factor operation. This inverter was tested again for the condition of injecting imbalanced currents, but in this case compensating also reactive loads. Figure 15 shows the waveforms of the three phase currents injected into the testing system and voltage and current of phase $L_1$. Through their analysis, it is possible to confirm that the currents are imbalanced and that they are not in phase anymore. It is possible to confirm the active and reactive compensation of the imbalanced loads.
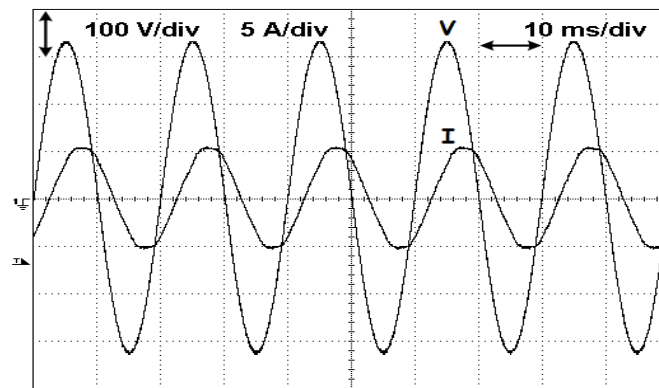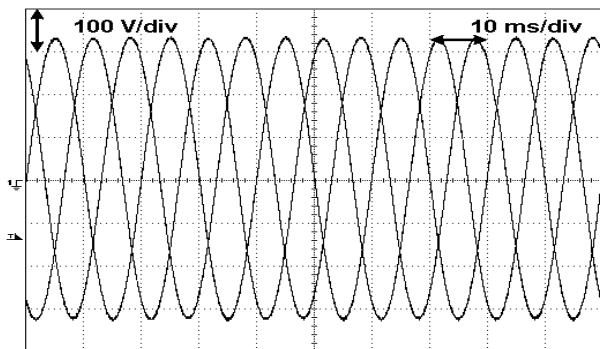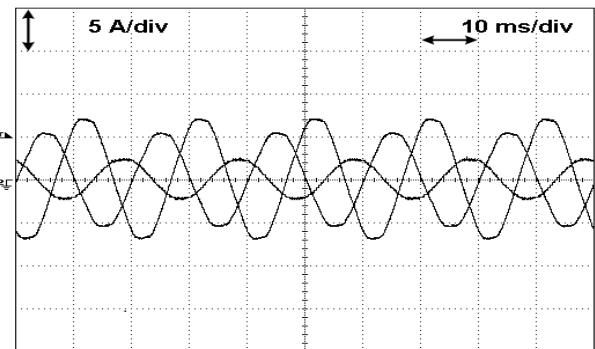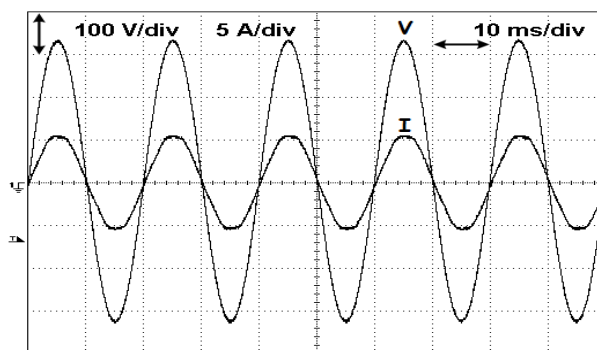


**Figure 13.** Waveforms of the voltage and current in phase $L_1$ of the testing system obtained from the test using the *PV* inverter with four legs for a balanced condition and with reactive compensation.



(**a**)



(**b**)



(**c**)

**Figure 14.** Waveforms obtained from the test using the *PV* inverter with four legs for an imbalanced condition and without reactive compensation: (**a**) three-phase voltages imposed by the testing system, (**b**) three-phase currents injected by the *PV* system, (**c**) voltage and current in phase $L_1$ of the testing system.
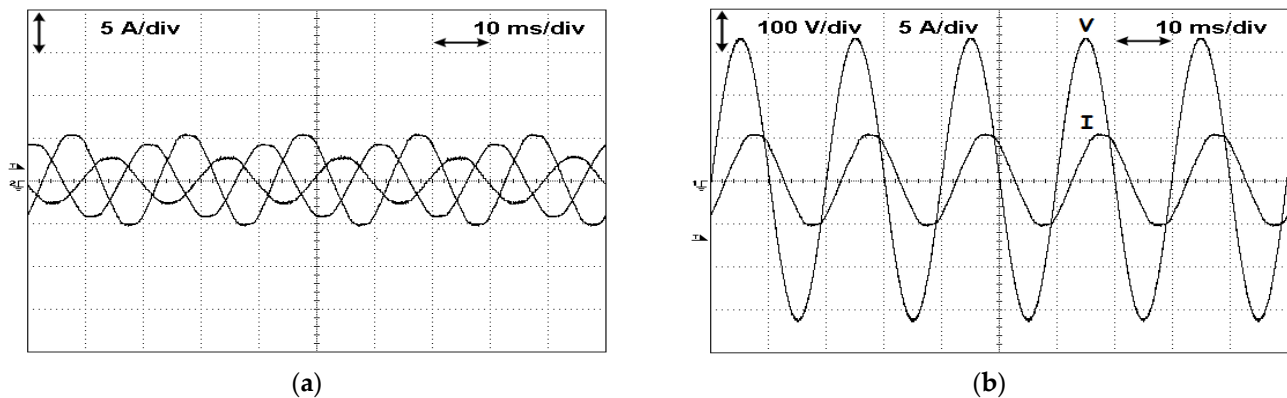
**Figure 15.** Waveforms obtained from the test using the *PV* inverter with four legs for an imbalanced condition and with reactive compensation: (**a**) three-phase currents injected by the *PV* system, (**b**) voltage and current in phase $L_1$ of the testing system.

## 6. Discussion

Due to the importance of the PV generators in the actual context of the renewable energy sources, the criteria to interconnect them into the electrical grid increases constantly. Thus, these kind of generators should be tested before their integration into the grid. Those tests must be in accordance with the applicable grid codes that exist in different countries. In fact, those rules usually differ from country to country, which is a strong barrier regarding grid-connected PV systems' large deployment. Nowadays, there are already testing systems for PV generators. However, they only allow for testing the generators for the existing applicable grid codes, and they are not adapted for new grid codes that can appear in the future or requirements from specific clients. This is the case of testing the PV inverters that allows giving support to the network under the perspective of the balance of low-voltage networks with neutral wire. For this kind of tests, there is the need for a testing system that supports a four-wire connection for the PV inverter. However, this is not the standard in the industry, since they typically only allow for a three-wire connection. Thus, this work proposes a solution that can be used in the future by the industry, based on classical converters such as the H-bridge inverters which allow for developing a low-cost testing system. This is an important aspect for a future industry application. In Table 3, several types of equipment can be seen that have already been developed for PV generators. As shown in that table, there are several different pieces of equipment that have been developed for this system. However, each of them is designed for a specific test, since there are different aspects that need to be tested. Nevertheless, one piece of test equipment that was not developed was for the test of the PV inverter, taking into consideration their capability to provide ancillary services requiring a neutral connection. Another important aspect is the control of the testing system. Many times, the controller presents a low dynamic, which could affect the test of the PV inverter under, for example, fast perturbations. This work also tried to focus on this. Finally, another aspect that is also important is that with the implementation of PV generators, new grid codes could appear in the near future. Thus, the testing system should be flexible enough to allow the implementation of tests taking into consideration these new grid codes. This is an aspect not considered in this work, since its purpose was more to have an approach under the perspective of the hardware of the testing system. Nevertheless, the software is also an important part that needs many resources.

**Table 3.** Comparison of the proposed PV generator testing system with other developed equipment.

| Characteristic     Equipment | [8] | [9] | [30] | [33] | Proposed |
|---|---|---|---|---|---|
| PV emulator | Yes | Yes | No | No | No |
| MPPT | Yes | Yes | No | No | No |
| Arc fault detector | No | No | Yes | No | No |
| Test Inverter | No | No | No | Yes | Yes |
| Test typical ancillary services | No | No | No | Yes | Yes |
| Test ancillary services requiring a neutral | No | No | No | No | Yes |

## 7. Conclusions

In this work, the design of a testing setup for grid-connected *PV* systems was presented and described. This setup was developed taking into consideration the last requirements and recommendations for the integration of *PV* systems in distribution grids (micro and smart grids frameworks). In this context, the standards and recommendations for the referred integrations were presented and considered. In accordance with those specifications, a controllable power source prepared to receive energy, as well as to inject it into the grid, was developed for the testing system. The capability of injecting energy into the grid has the purpose of testing *PV* systems with storage devices. The power converters of the system allow for imposing a controllable voltage, in amplitude and frequency, to the *PV* system. In this way, it will be possible to simulate the perturbations of the grid. Two power converters were used, namely a four-leg voltage source inverter with an *LC* filter to connect to the *PV* system and a three-phase power factor corrector connected to the grid. To choose the test that will be imposed to the *PV* system, the setup is connected to a laptop. In this laptop, there is a program that generates the references for the control system of the power converter and in which the user defines the test to be performed. Several experimental tests were obtained, in which a commercial solar inverter and a *PV* generator developed in the context of a European project, were used. The results showed the characteristics and capabilities of the developed testing system. Due to those capabilities, it was possible to verify that the setup gives an easy and flexible way to test *PV* systems in accordance with the latest requirements and recommendations. One aspect not considered in the work is the software, since the purpose was more to have an approach under the perspective of the hardware of the testing system. However, the software is also an important part due to the fact that in the near future, new grid codes could appear. In this way, a perspective of further research is the development of the components' software, especially taking into consideration the possibility of testing the PV generators under new grid codes that eventually could appear.

**Author Contributions:** Conceptualization, V.F.P., H.C. and J.F.M.; methodology, V.F.P. and H.C.; simulations, V.F.P. and J.F.M.; validation, V.F.P., D.F., A.C. and A.P.; formal analysis, V.F.P. and J.F.M.; investigation, V.F.P.; resources, V.F.P.; data curation, V.F.P.; writing—original draft preparation V.F.P., D.F. and A.C.; writing—review and editing, A.P. and A.C.; visualization, A.P. and A.C.; supervision, A.P.; project administration, J.F.M.; funding acquisition, A.P. and J.F.M. All authors have read and agreed to the published version of the manuscript.

# References

1. Gielen, D.; Boshell, F.; Saygin, D.; Bazilian, M.D.; Wagner, N.; Gorini, R. The role of renewable energy in the global energy transformation. *Energy Strategy Rev.* **2019**, *40*, 38–50. [CrossRef]
2. International Energy Agency. Renewables 2022: Analysis and Forecasts to 2027. Available online: https://www.iea.org/reports/renewables-2022 (accessed on 6 February 2023).
3. Rehman, A.; Radulescu, M.; Cismas, L.M.; Alvarado, R.; Secara, C.G.; Tolea, C. Urbanization, Economic Development, and Environmental Degradation: Investigating the Role of Renewable Energy Use. *Sustainability* **2022**, *14*, 9337. [CrossRef]
4. Strasser, T.; Andrén, F.; Kathan, J.; Cecati, C.; Buccella, C.; Siano, P.; Leitão, P.; Zhabelova, G.; Vyatkin, V.; Vrba, P. A Review of Architectures and Concepts for Intelligence in Future Electric Energy Systems. *IEEE Trans. Ind. Electron.* **2015**, *62*, 2424–2438. [CrossRef]
5. Kavya Santhoshi, B.; Mohana Sundaram, K.; Padmanaban, S.; Holm-Nielsen, J.B. Critical Review of PV Grid-Tied Inverters. *Energies* **2019**, *12*, 1921. [CrossRef]
6. Gupta, N.; Dogra, R.; Garg, R.; Kumar, P. Review of islanding detection schemes for utility interactive solar photovoltaic systems. *Int. J. Green Energy* **2022**, *19*, 242–253. [CrossRef]
7. Rangarajan, S.S.; Collins, E.R.; Fox, J.C.; Kothari, D.P. A survey on global PV interconnection standards. In Proceedings of the IEEE Power and Energy Conference at Illinois (PECI), Champaign, IL, USA, 23–24 February 2017; pp. 1–8.
8. Jin, S.; Zhang, D.; Bao, Z.; Liu, X. High Dynamic Performance Solar Array Simulator Based on a SiC MOSFET Linear Power Stage. *IEEE Trans. Power Electron.* **2018**, *33*, 1682–1695. [CrossRef]
9. Moussa, I.; Khedher, A.; Bouallegue, A. Design of a Low-Cost PV Emulator Applied for PVECS. *Electronics* **2019**, *8*, 232. [CrossRef]
10. Sanaullah, S.; Khan, H.A. Design and implementation of a low cost Solar Panel emulator. In Proceedings of the IEEE 42nd Photovoltaic Specialist Conference (PVSC), New Orleans, LA, USA, 14–19 June 2015; pp. 1–5.
11. Korasiak, P.; Jaglarz, J.A. New Photovoltaic Emulator Designed for Testing Low-Power Inverters Connected to the LV Grid. *Energies* **2022**, *15*, 2646. [CrossRef]
12. Ahmed, M.; Harbi, I.; Kennel, R.; Abdelrahem, M. Maximum Power Point Tracking Implementation under Partial Shading Conditions Using Low-Cost Photovoltaic Emulator. *Energy* **2022**, *3*, 424–438. [CrossRef]
13. Chen, C.-C.; Chang, H.-C.; Kuo, C.-C.; Lin, C.-C. Programmable energy source emulator for photovoltaic panels considering partial shadow effect. *Energy* **2013**, *54*, 174–183. [CrossRef]
14. Merenda, M.; Iero, D.; Carotenuto, R.; Della Corte, F.G. Simple and Low-Cost Photovoltaic Module Emulator. *Electronics* **2019**, *8*, 1445. [CrossRef]
15. Prasanth Ram, J.; Manghani, H.; Dhanup, S.; Pillai, T.; Babu, S.; Miyatake, M.; Rajasekar, N. Analysis on solar PV emulators: A review. *Renew. Sustain. Energy Rev.* **2018**, *81*, 149–160.
16. Schofield, D.M.K.; Foster, M.P.; Stone, D.A. Low-cost solar emulator for evaluation of maximum power point tracking methods. *Electron. Lett.* **2011**, *47*, 208–209. [CrossRef]
17. Ma, C.-T.; Tsai, Z.-Y.; Ku, H.-H.; Hsieh, C.-L. Design and Implementation of a Flexible Photovoltaic Emulator Using a GaN-Based Synchronous Buck Converter. *Micromachines* **2021**, *12*, 1587. [CrossRef]
18. Jayawardana, I.D.G.; Ho, C.N.M.; Pokharel, M.; Valderrama, G.E. A Fast-Dynamic Control Scheme for a Power-Electronics-Based PV Emulator. *IEEE J. Photovolt.* **2021**, *11*, 485–495. [CrossRef]
19. Ayop, R.; Tan, C.W. Rapid Prototyping of Photovoltaic Emulator Using Buck Converter Based on Fast Convergence Resistance Feedback Method. *IEEE Trans. Power Electron.* **2019**, *34*, 8715–8723. [CrossRef]
20. Cordeiro, A.; Foito, D.; Pires, V.F. A PV panel simulator based on a two quadrant DC/DC power converter with a sliding mode controller. In Proceedings of the International Conference on Renewable Energy Research and Applications, Palermo, Italy, 22–25 November 2015; pp. 928–932.
21. Premkumar, M.; Jangir, P.; Sowmya, R.; Rajvikram Elavarasan, M.; Kumar, B.S. Enhanced chaotic JAYA algorithm for parameter estimation of photovoltaic cell/modules. *ISA Trans.* **2021**, *116*, 139–166. [CrossRef] [PubMed]
22. Batzelis, E. Non-Iterative Methods for the Extraction of the Single-Diode Model Parameters of Photovoltaic Modules: A Review and Comparative Assessment. *Energies* **2019**, *12*, 358. [CrossRef]
23. Shinde, U.K.; Kadwane, S.G.; Gawande, S.P.; Keshri, R. Solar PV emulator for realizing PV characteristics under rapidly varying environmental conditions. In Proceedings of the IEEE International Conference on Power Electronics, Drives and Energy Systems, Trivandrum, India, 14–17 December 2016; pp. 1–5.
24. Fahim, S.R.; Hasanien, H.M.; Turky, R.A.; Aleem, S.H.E.A.; Ćalasan, M. A Comprehensive Review of Photovoltaic Modules Models and Algorithms Used in Parameter Extraction. *Energies* **2022**, *15*, 8941. [CrossRef]
25. Raya-Armenta, J.M.; Ortega, P.R.; Bazmohammadi, N.; Spataru, S.V.; Vasquez, J.C.; Guerrero, J.M. An Accurate Physical Model for PV Modules with Improved Approximations of Series-Shunt Resistances. *IEEE J. Photovolt.* **2021**, *11*, 699–707. [CrossRef]
26. Kihal, A.; Krim, F.; Laib, A.; Talbi, B.; Afghoul, H. An improved MPPT scheme employing adaptive integral derivative sliding mode control for photovoltaic systems under fast irradiation changes. *ISA Trans.* **2019**, *87*, 297–306. [CrossRef]
27. Villalva, M.G.; Gazoli, J.R.; Filho, E.R. Comprehensive Approach to Modeling and Simulation of Photovoltaic Arrays. *IEEE Trans. Power Electron.* **2009**, *24*, 1198–1208. [CrossRef]
28. Sheikhipour, S.; Ghadimi, A.A.; Mirzaei, A. A sensor-less control and optimal energy management algorithm for a stand-alone photovoltaic system considering partial shading condition. *ISA Trans.* **2021**, *128*, 606–623. [CrossRef] [PubMed]

29. Mahmoud, Y.; Xiao, W.; Zeineldin, H.H. A Simple Approach to Modeling and Simulation of Photovoltaic Modules. *IEEE Trans. Sustain. Energy* **2012**, *3*, 185–186. [CrossRef]

30. Ameen, R.; Abdulmawjood, K.; Abbas, S.; Shukri, S.; Khraisheh, K.; Alpuerto, L.; Balog, R.S. Mechatronics Arc Generator for Photovoltaic Arc Fault Detector Testing. In Proceedings of the IEEE 46th Photovoltaic Specialists Conference (PVSC), Chicago, IL, USA, 16–21 June 2019; pp. 1306–1311. [CrossRef]

31. Kim, K.A.; Xu, C.; Jin, L.; Krein, P.T. A Dynamic Photovoltaic Model Incorporating Capacitive and Reverse-Bias Characteristics. *IEEE J. Photovolt.* **2013**, *3*, 1334–1341. [CrossRef]

32. Vogel, S.; Nguyen, H.T.; Stevic, M.; Jensen, T.V.; Heussen, K.; Rajkumar, V.S.; Monti, A. Distributed Power Hardware-in-the-Loop Testing Using a Grid-Forming Converter as Power Interface. *Energies* **2020**, *13*, 3770. [CrossRef]

33. Si, G.; Cordier, J.; Kennel, R.M. Extending the Power Capability with Dynamic Performance of a Power-Hardware-in-the-Loop Application-Power Grid Emulator Using Inverter Cumulation. *IEEE Trans. Ind. Appl.* **2016**, *52*, 3193–3202. [CrossRef]

34. Hildebrandt, N.; Luo, M.; Dujic, D. Robust and Cost-Effective Synchronization Scheme for a Multicell Grid Emulator. *IEEE Trans. Ind. Electron.* **2021**, *68*, 1851–1859. [CrossRef]

35. Wang, J.; Yang, L.; Ma, Y.; Wang, J.; Tolbert, L.M.; Wang, F.; Tomsovic, K. Static and dynamic power system load emulation in a converter-based reconfigurable power grid emulator. *IEEE Trans. Power Electron.* **2016**, *31*, 3239–3251. [CrossRef]

36. Ahmad, Z.; Torres, J.R.; Kumar, V.N.; Rakhshani, E.; Palensky, P.; Meijden, M. A Power Hardware-in-the-Loop Based Method for FAPR Compliance Testing of the Wind Turbine Converters Control. *Energies* **2020**, *13*, 5203. [CrossRef]

37. Pires, V.F.; Martins, L.S.; Amaral, T.G.; Marçal, R.; Rodrigues, R.; Crisóstomo, M.M. Distance Learning Power System Protection Based on Testing Protective Relays. *IEEE Trans. Ind. Electron.* **2008**, *55*, 2433–2438. [CrossRef]

38. Collins, E.R.; Morgan, R.L. A three-phase sag generator for testing industrial equipment. *IEEE Trans. Power Deliv.* **1996**, *11*, 526–532. [CrossRef]

39. Bielemeier, J.; Frehn, A.; Monti, A.; Frühmann, R.; Santjer, F. Comparison of multi-megawatt LVRT testing setups for the certification of wind turbines. In Proceedings of the IEEE Milan PowerTech, Milan, Italy, 23–27 June 2019; pp. 1–6.

40. Mesbah, M.; Moses, P.S.; Islam, S.M.; Masoum, M.A.S. Digital Implementation of a Fault Emulator for Transient Study of Power Transformers Used in Grid Connection of Wind Farms. *IEEE Trans. Sustain. Energy* **2014**, *5*, 646–654. [CrossRef]

41. Biligiri, K.; Harpool, S.; Jouanne, A.; Amon, E.; Brekken, T. Grid emulator for compliance testing of Wave Energy Converters. In Proceedings of the IEEE Conference on Technologies for Sustainability, Portland, OR, USA, 24–26 July 2014; pp. 30–34.

42. Zeb, K.; Uddin, W.; Adil Khan, M.; Ali, Z.; Umair Ali, M.; Christofides, N.; Kim, H.J. A comprehensive review on inverter topologies and control strategies for grid connected photovoltaic system. *Renew. Sustain. Energy Rev.* **2018**, *94*, 1120–1141. [CrossRef]

43. Mohamed Hariri, M.H.; Mat Desa, M.K.; Masri, S.; Mohd Zainuri, M.A.A. Grid-Connected PV Generation System—Components and Challenges: A Review. *Energies* **2020**, *13*, 4279. [CrossRef]

44. Fernão Pires, V.; Cordeiro, A.; Foito, D.; Pires, A.J.; Hao, C.; Martins, J.F.; Castro, R. Compensation of Unbalanced Low-Voltage Grids Using a Photovoltaic Generation System with a Dual Four-Leg, Two-Level Inverter. *Electronics* **2022**, *11*, 320. [CrossRef]

45. Shahparasti, M.; Savaghebi, M.; Adabi, E.; Ebel, T. Dual-Input Photovoltaic System Based on Parallel Z-Source Inverters. *Designs* **2020**, *4*, 51. [CrossRef]

46. Ali Khan, M.Y.; Liu, H.; Yang, Z.; Yuan, X. A Comprehensive Review on Grid Connected Photovoltaic Inverters, Their Modulation Techniques, and Control Strategies. *Energies* **2020**, *13*, 4185. [CrossRef]

47. Hassan, Z.; Amir, A.; Selvaraj, J.; Rahim, N.A. A review on current injection techniques for low-voltage ride-through and grid fault conditions in grid-connected photovoltaic system. *Sol. Energy* **2020**, *207*, 851–873. [CrossRef]

48. Ahmed, M.; Harbi, I.; Kennel, R.; Rodríguez, J.; Abdelrahem, M. Evaluation of the Main Control Strategies for Grid-Connected PV Systems. *Sustainability* **2022**, *14*, 11142. [CrossRef]

49. Verbytskyi, I.; Lukianov, M.; Nassereddine, K.; Pakhaliuk, B.; Husev, O.; Strzelecki, R.M. Power Converter Solutions for Industrial PV Applications—A Review. *Energies* **2022**, *15*, 3295. [CrossRef]

50. Haq, S.; Biswas, S.P.; Hosain, M.K.; Rahman, M.A.; Islam, M.R.; Jahan, S. A Modular Multilevel Converter with an Advanced PWM Control Technique for Grid-Tied Photovoltaic System. *Energies* **2021**, *14*, 331. [CrossRef]

51. Medina-García, J.; Martín, A.D.; Cano, J.M.; Gómez-Galán, J.A.; Hermoso, A. Efficient Wireless Monitoring and Control of a Grid-Connected Photovoltaic System. *Appl. Sci.* **2021**, *11*, 2287. [CrossRef]

52. Zeb, K.; Islam, S.U.; Khan, I.; Uddin, W.; Ishfaq, M.; Busarello, S.M.; Muyeen, I.A.; Kim, H.J. Faults and Fault Ride through strategies for grid-connected photovoltaic system: A comprehensive review. *Renew. Sustain. Energy Rev.* **2022**, *158*, 112125. [CrossRef]

53. Zhiyong, Y.; Guangbin, L.; Hong, W. Development of generator for voltage dips, short interruptions and voltage variations immunity test. In Proceedings of the 3rd International Symposium on Electromagnetic Compatibility, Beijing, China, 21–24 May 2002; pp. 67–70.

54. Callegaro, L.; Konstantinou, G.; Rojas, C.A.; Avila, N.F.; Fletcher, J.E. Testing Evidence and Analysis of Rooftop PV Inverters Response to Grid Disturbances. *IEEE J. Photovolt.* **2020**, *10*, 1882–1891. [CrossRef]

55. Wu, Y.; Lin, J.; Lin, H. Standards and Guidelines for Grid-Connected Photovoltaic Generation Systems: A Review and Comparison. *IEEE Trans. Ind. Appl.* **2017**, *53*, 3205–3216. [CrossRef]

56. Crăciun, B.; Kerekes, T.; Séra, D.; Teodorescu, R. Overview of recent Grid Codes for PV power integration. In Proceedings of the 13th International Conference on Optimization of Electrical and Electronic Equipment (OPTIM), Brasov, Romania, 24–26 May 2012; pp. 959–965.

57. Al-Shetwi, A.Q.; Hannan, M.A.; Jern, K.P.; Alkahtani, A.A.; PGAbas, A.E. Power Quality Assessment of Grid-Connected PV System in Compliance with the Recent Integration Requirements. *Electronics* **2020**, *9*, 366. [CrossRef]

58. Abubakr, H.; Vasquez, J.C.; Mahmoud, K.; Darwish, M.M.F.; Guerrero, J.M. Comprehensive Review on Renewable Energy Sources in Egypt—Current Status, Grid Codes and Future Vision. *IEEE Access* **2022**, *10*, 4081–4410. [CrossRef]

59. Power Generation Systems Connected to the Low-Voltage Distribution Network—Technical Minimum Requirements for the Connection to and Parallel Operation with Low-Voltage Distribution Networks. In *Association for Electrical, Electronic & Information Technologies*; VDE-AR-N 4105-2011; VDE Publishing House: Berlin, Germany, 2011.

60. Weckx, S.; Gonzalez, C.; Driesen, J. Reducing grid losses and voltage unbalance with PV inverters. In Proceedings of the IEEE PES General Meeting Conference & Exposition, National Harbor, MD, USA, 27–31 July 2014; pp. 1–5.

61. O'Rourke, C.J.; Qasim, M.M.; Overlin, M.R.; Kirtley, J.L. A Geometric Interpretation of Reference Frames and Transformations: dq0, Clarke, and Park. *IEEE Trans. Energy Convers.* **2019**, *34*, 2070–2083. [CrossRef]

62. Gao, W.; Hung, J.C. Variable structure control of nonlinear systems: A new approach. *IEEE Trans. Ind. Electron.* **1993**, *40*, 45–55. [CrossRef]

63. Havrlík, M.; Libra, M.; Poulek, V.; Kouřím, P. Analysis of Output Signal Distortion of Galvanic Isolation Circuits for Monitoring the Mains Voltage Waveform. *Sensors* **2022**, *22*, 7769. [CrossRef] [PubMed]

64. Al-Shetwi, A.Q.; Sujod, M.Z.; Blaabjerg, F.; Yang, Y. Fault ride-through control of grid-connected photovoltaic power plants: A review. *Sol. Energy* **2019**, *180*, 340–350. [CrossRef]